U.S. Geological Survey Final Technical Report

Award No. G14AP00006
Recipient: University of California at Santa Barbara

Continuing to Map the 3D Geometry of Active Faults in Southern California

Craig Nicholson[1], Andreas Plesch[2], Christopher Sorlien[3], John Shaw[2]
& Egill Hauksson[4]
[1]*Marine Science Institute, UC Santa Barbara*
[2]*Department of Earth & Planetary Sciences, Harvard University*
[3]*Earth Research Institute, UC Santa Barbara*
[4]*Seismological Laboratory, California Institute of Technology*

Principal Investigator: Craig Nicholson
Marine Science Institute, University of California
MC 6150, Santa Barbara, CA 93106-6150
phone: 805-893-8384; fax: 805-893-8062; email: nicholson@msi.ucsb.edu

01 December 2013 - 31 May 2015

Research supported by the U.S. Geological Survey (USGS), Department of the Interior, under USGS Award No. **G14AP00006**. The views and conclusions contained in this document are those of the authors, and should not be interpreted as necessarily representing the official policies, either expressed or implied, of the U.S. Government.

Continuing to Map the 3D Geometry of Active Faults in Southern California

Abstract

Accurate assessment of the earthquake and tsunami hazard in southern California requires an accurate and complete description of the active onshore and offshore faults in three dimensions. Many aspects of seismic hazard evaluation, including developing credible earthquake rupture scenarios, predicting strong ground motion, estimating tsunami runup heights, or modeling geodetic and geologic fault slip rates and the mechanical behavior of faults are all strongly dependent on accurately resolving the 3D geometry of active faults at seismogenic depths. Having accurate and realistic 3D models of subsurface fault geometry is also particularly important when investigating the likelihood of multi-fault ruptures in southern California, or resolving the influence of fault complexity on the distribution of surface uplift, or on dynamic earthquake rupture models. Because of this, the Southern California Earthquake Center and the US Geological Survey Earthquake Hazards Program have consistently targeted the testing and development of new, updated 3D fault models for southern California as a primary research objective. The purpose of this project was to continue to provide just such improved, more detailed and more realistic, updated 3D fault representations for input into the SCEC Community Fault Model (CFM).

Thus, as part of the on-going effort to systematically update and improve CFM, and working in close collaboration with various members of the CFM Working Group, steady and significant improvements to CFM and its associated fault database were made [*Nicholson et al.,* 2014, 2015; *Plesch et al.,* 2014]. These improvements include new, more complex 3D fault surfaces based on detailed fault surface trace, industry well, seismic reflection, relocated hypocenter and focal mechanism nodal plane data, and an updated fault database with an improved hierarchical fault naming and numbering system. The results document a wide variety of complex fault deformation styles, including: various aspects of strain partitioning and fault-related folding; sets of both high-angle and low-angle faults that mutually interact; blind and emergent structures; significant non-planar, multi-stranded faults with variable dip along strike and with depth; and active mid-crustal detachments at different structural levels. In places, closely-spaced fault strands or fault systems can remain surprisingly subparallel to seismogenic depths, while in other areas, major strike-slip to oblique-slip faults can merge or diverge with depth. The updated CFM 3D fault surfaces thus help characterize a more complex pattern of fault interactions at depth between various fault sets and linked fault systems, and a more complex fault geometry than typically inferred or expected from projecting near-surface geologic or geophysical data down-dip.

In 2014, the formally reviewed and ranked CFM 4.0 and its rectilinear version were released, along with an initial CFM Version 5.0. In addition to continuing to update older fault models, many new faults or alternative representations were added to CFM 5.0 that were not represented in any previous CFM model versions. This included faults in the onshore Santa Maria basin, Eastern and Western Transverse Ranges, Mojave, various offshore fault systems, and faults within the designated San Gorgonio Pass and Ventura Special Fault Study Areas. The net result is that CFM 5.0 now contains 90 separate fault zones or distinct fault systems defined by over 300 individual named faults, with 325 new, updated, or revised fault models or alternative representations added to CFM since Version 3.0. CFM 5.0 is provided as a series of digital, triangulated fault surfaces, and is available on-line from the SCEC-CFM webpage accessible from the structure.harvard.edu website.

Introduction

Accurate assessment of the earthquake hazards in southern California requires accurate and complete 3D fault maps. Many aspects of seismic hazard evaluation, including understanding earthquake rupture and geodetic strain, developing credible earthquake rupture scenarios, modeling geodetic and geologic fault slip rates, or predicting strong ground motion, are all strongly dependent on accurately resolving the 3D geometry of active faults at seismogenic depths [*Herbert and Cooke*, 2012; *Lindsey et al.,* 2012, *Oglesby and Mai*, 2012; *Shi et al.,* 2012; *Lozos et al.,* 2013; *Trugman and Dunham,* 2013; *Fattaruso et al.,* 2014; *Marshall et al.,* 2013, 2014; *Shi,* 2014; *Ryan et al.,* 2015]. In southern California, these structures can be quite complex and include both relatively high-angle strike-slip and oblique-slip faults—many of which intersect and are mapped at the surface, as well as low-to-moderate-angle faults, some of which are blind and are difficult to identify. The 1994 M6.7 Northridge earthquake was on one such blind fault and produced over $40 billion in damage. Because of this, both the Southern California Earthquake Center (SCEC) and US Geological Survey EHP have consistently targeted the identification and mapping in 3D of active faults in southern California as a primary research objective. The purpose of this project was to continue to provide just such improved, more detailed, updated 3D fault representations for input into the online SCEC Community Fault Model (CFM) by allowing for an expanded research effort in areas of complex fault geometry and fault interaction.

Thus, as part of the on-going, multi-year effort within SCEC to systematically update and improve CFM, and working in close collaboration with Andreas Plesch, Chris Sorlien, John Shaw, Egill Hauksson and other members of the CFM Working Group, steady and significant improvements to CFM and its associated fault database were made [e.g., *Nicholson et al.,* 2014; *Plesch et al.,* 2014; *Shaw et al.,* 2015]. These improvements include new, more complex and realistic 3D representations of major active faults (**Fig.1**), more detailed fault surface trace data, and a new hierarchical naming and numbering scheme for CFM that allows for closer links to the USGS Quaternary fault (Qfault) database. In 2014, the formal, ranked CFM 4.0 and its rectilinear version were released, along with an initial CFM Version 5.0. In addition to updating older Version 3.0 fault models, many new faults or alternative representations were added to CFM 5.0 that were not represented in any previous CFM model versions. This included faults in the onshore Santa Maria basin, Eastern & Western Transverse Ranges, Mojave, various offshore fault systems, and faults within the designated San Gorgonio Pass and Ventura Special Fault Study Areas (SFSA). The net result is that CFM 5.0 now contains 90 separate fault zones or distinct fault systems defined by over 300 individual named faults, with 325 new, updated, or revised fault models added to CFM since Version 3.0 (**Fig.1**)[*Nicholson et al.,* 2014; 2015; *Plesch et al.,* 2014].

The advantage of these new models is that they allow for more non-planar, multi-stranded 3D fault geometry, including more variability in dip along strike and with depth. The new models are more consistent with alignments of relocated hypocenters and focal mechanism nodal planes, and have a higher concentration of hypocenters within close proximity (±1 km) of the modeled 3D slip surface [*Hauksson*, 2012; *Hauksson et al*., 2013] than previous CFM 3.0 fault models (**Fig.1**). The new 3D fault models also help characterize a more detailed and complex pattern of fault interactions at depth between various fault sets and linked fault systems, and may thus help to explain some of the more enigmatic fault behavior that is otherwise difficult to understand.

In addition to updating 3D fault models for CFM, we have also finalized a new CFM fault database hierarchical naming and numbering scheme. This allows CFM to properly organize, name and number the increasing variety and complexity of modeled, multi-stranded principal slip surfaces and associated secondary faults, while maintaining more consistency with fault nomenclature from the CGS Fault Activity and USGS Quaternary Fault database systems.

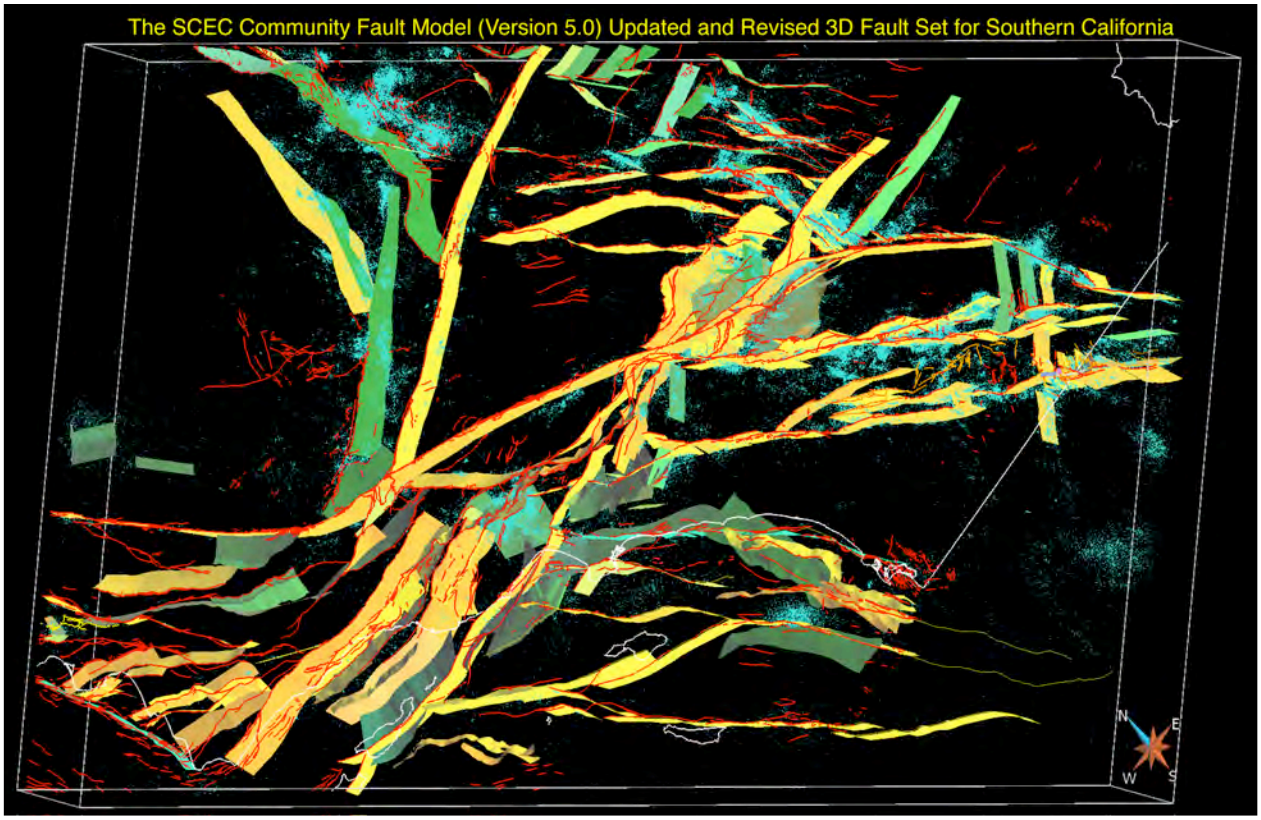

Figure 1. Oblique 3D view looking NE of new or updated CFM 5.0 fault models, plus USGS/CGS fault surface traces (red lines), and relocated seismicity (blue dots) [*Nicholson et al*., 2014; *Plesch et al*., 2014]. CFM 5.0 improvements include 190 new, updated or revised 3D fault models or alternative representations added to CFM since the release of CFM 4.0, or a total of 325 new or updated faults (orange to yellow surfaces) added to CFM since 2011 and to the remaining CFM 3.0 fault models (green surfaces). Seismicity from *Hauksson et al*. [2012].

Data and Methods

The primary data sets used in this and related SCEC projects are the most recent, revised catalogs of relocated earthquake hypocenters and earthquake focal mechanism solutions [*Hauksson et al*., 2012; *Yang et al*., 2012], plus USGS Digital Elevation Models of surface topography, and mapped Quaternary fault surface traces (Qfault)[*Bryant,* 2005; *USGS*, 2006]. All of these data sets are readily available online. The revised earthquake hypocenters were calculated using a procedure that involved initial relocations with absolute travel-times, source-specific station terms and a 3D velocity model, waveform cross-correlation to improve clustering and identify related earthquake pairs, and differential travel times from cross-correlated pairs to determine relative relocation within clusters [*Hauksson and Shearer,* 2005; *Shearer et al*., 2005; *Lin et al*., 2007; *Hauksson et al*., 2012]. Focal mechanisms were then determined from these revised earthquake hypocenters using both P-wave first-motions and S/P amplitude ratios [*Hardebeck and Shearer*, 2003; *Yang et al*., 2012]. For faults associated with the recent 2010 El Mayor-Cucapah sequence, the Laguna Salada fault zone, or found in the Sierra Cucapah and Yuha Desert area, we had supplemental fault surface trace maps and InSAR fault models courtesy of John Fletcher, Ken Hudnut, Jerry Treiman, and Mike Oskin [e.g., *Fletcher et al*., 2010; *Treiman et al*., 2010; *Teran et al*., 2011; *Oskin et al*., 2012].

For active faults located offshore in the California Borderland, both deep-penetration multi-channel seismic (MCS) (**Fig.2**) and high-resolution reflection lines from 2D and 3D seismic surveys were used to help map 3D fault surfaces and dated stratigraphic references horizons in the shallow crust [*Sorlien and Kamerling,* 2000; *Kamerling et al*., 2003; *Sorlien et al*., 2014; 2015].

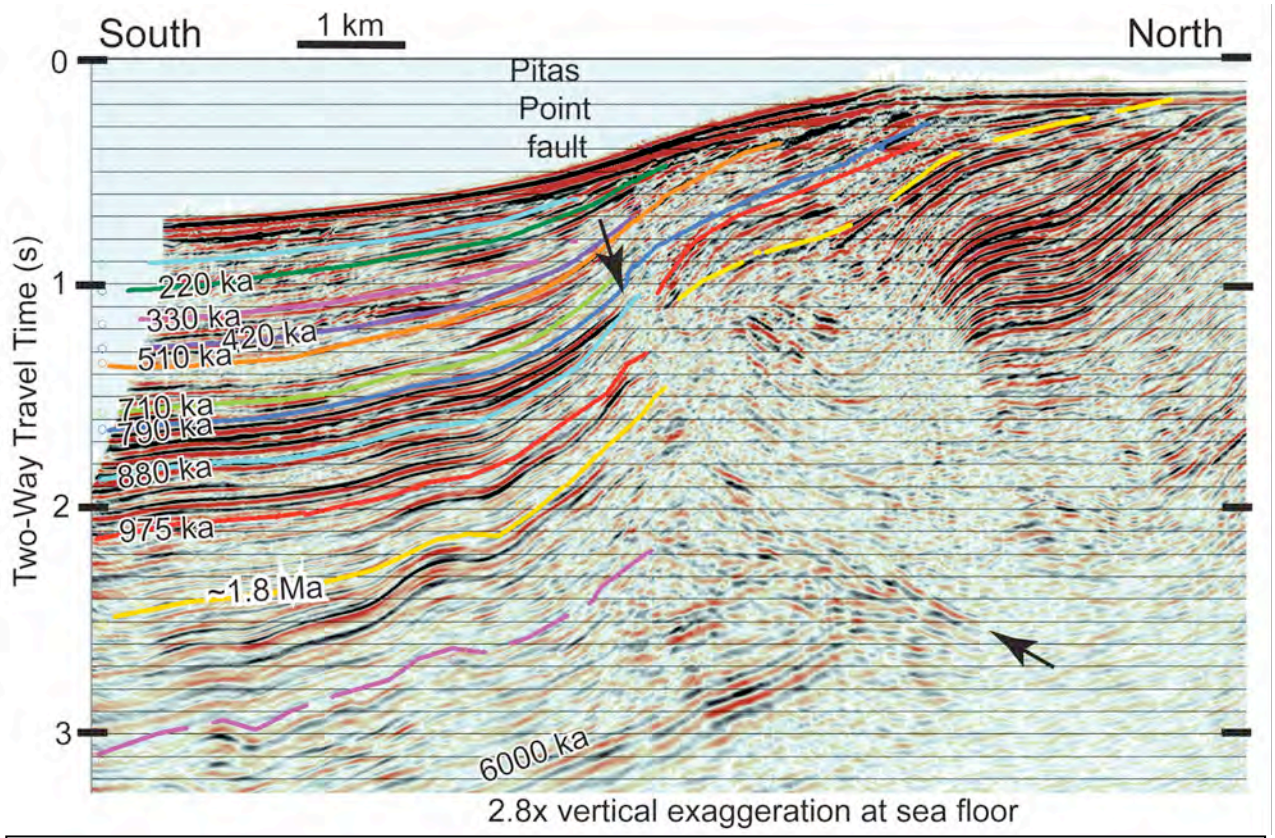

Figure 2. Example of industry marine MCS reflection profile from the Gato Canyon 3D seismic survey (in-line 10) used to help map shallow offshore 3D fault surfaces, like the Pitas Point fault (arrows), and dated stratigraphic reference hoizons [*Sorlien et al.,* 2014]. Yellow is top Lower Pico (~1.8 Ma).

In addition, sets of surface geologic maps, interpreted geologic cross sections and subsurface structure contour maps of stratigraphic reference horizons were used where available to help define near-surface and subsurface fault geometry in the shallow section that often exhibits little or no seismicity. These maps and cross sections are based on integrated correlations of surface geologic mapping, industry well logs and seismic reflection data [*c.f., Yeats et al,* 1977; *Yeats,* 1987, 2001; *Wright,* 1991; *Hopps et al.,* 1992; *Huftile and Yeats,* 1995; *Tsutsumi and Yeats,* 1999] and can often provide geologic control of subsurface fault geometry to depths of 3 to 4 km. Similar geological and geophysical data sets, as well as maps and cross sections are also available for offshore structures [c.f., *Kamerling et al.,* 1998, 2003; *Sorlien and Kamerling*, 2000; *Sorlien et al.*, 1998, 2000, 2006, 2013, 2015; *Redin et al.*, 2005; *Nicholson et al.,* 2007, 2011; *Marshall et al.,* 2012], and were used to generate digital 3D fault models for inclusion in CFM (**Fig.1**) [*Kamerling et al.,* 2001; *Schindler et al.,* 2007; *Bennett et al.,* 2012; *Sorlien et al.,* 2014, 2015]. Many of these once proprietary industry well files and seismic reflection data sets are now publicly available on-line or by request from DOGGR (http://owr.conservation.ca.gov/WellSearch/WellSearch.aspx for well files), USGS (http://walrus.wr.usgs.gov/NAMSS/ for marine seismic reflection data) and BOEMRE.

The basic procedure we use is actually quite simple. We start with the earthquake hypocenters and look for alignments in map, cross section or in 3D that define discrete principal slip surfaces (**Fig.3**, top). These surfaces can be planar or non-planar. We then overlay the earthquake focal mechanisms (**Fig.3,** bottom), but generally plot only one of the two possible nodal planes and the associated slip vector (inset) [*Seeber and Armbruster,* 1995]. If the alignment of the dominant focal mechanism nodal planes is consistent with the alignment of hypocenters, then the principal slip surface is considered well resolved. Generally, the best orientation for identifying such principal

slip surfaces is to look in 3D down-dip or along strike in the plane of slip for the fault. For active faults with shallow surfaces previously defined by industry MCS data (e.g., **Fig.2**), the deeper fault surface defined by seismicity is then matched to this shallow fault surface to insure continuity.

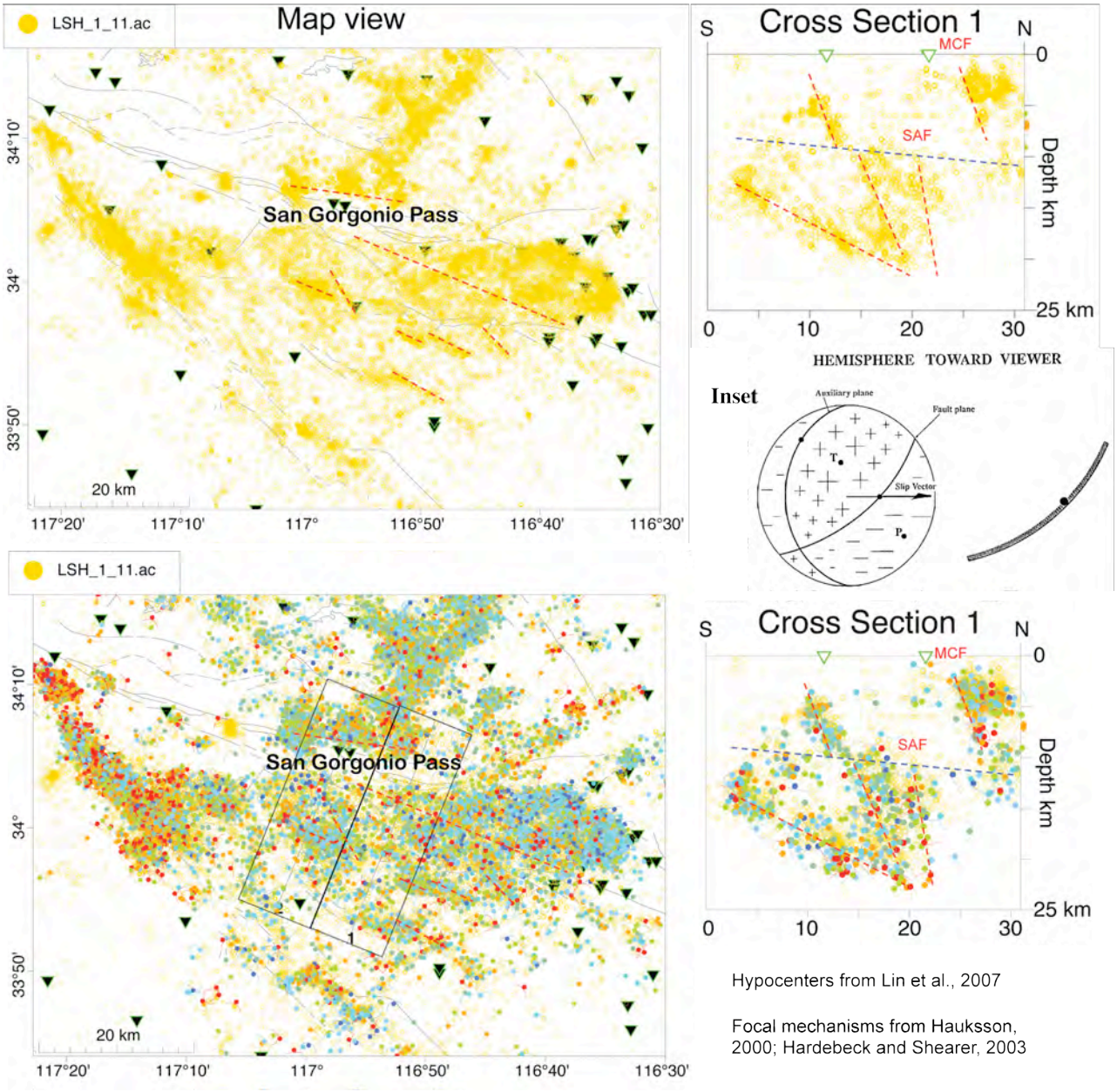

Figure 3. (top) Map and cross section of relocated hypocenters [*Lin et al.*, 2007] for the region around San Gorgonio Pass. Linear trends in hypocenter alignment denoted by dashed red lines; boundary between upper and lower crustal deformation shown by dashed blue line. Some older fault strands, like the Mill Creek fault (MCF) are best defined by where they truncate adjacent seismicity. (bottom) Map and cross section with overlay of single nodal planes and associated slip vectors (**inset**, *Seeber and Armbruster,* 1995). Note that a steeply dipping through-going predominantly strike-slip active strand of the San Andreas fault (SAF) can be defined through San Gorgonio Pass based on the alignment of earthquake hypocenters and focal mechansim nodal planes, but generally at depths below ~10 km.

Digital 3D fault surfaces were then generated in several ways, depending on the available data, and the quality and distribution of the hypocenters and nodal planes. If the hypocenters could define a discrete slip surface with non-planar fault geometry, a best-fitting gridded surface with varying

smoothing constraints was constructed with these events. If the events only defined a general linear trend, then a best-fitting median plane was constructed through the earthquake distribution. Faults with a mapped surface traces were generally constructed by projecting a smoothed version of the surface trace to depth, but with changing dip and fault geometry along strike, that best matched the changing geometry of discrete hypocenter clusters or dip of the predominant nodal plane (**Figs.4-6**).

This kinematic technique of using the spatial distribution of earthquake hypocenters and focal mechanisms to define the geometry of active subsurface faults has proven to be very effective in southern California [*Nicholson et al.,* 1986; *Nicholson and Seeber,* 1989; *Seeber and Armbruster,* 1995; *Carena et al.,* 2004]. The power of this technique lies in the internal consistency between two relatively independent datasets: (1) the spatial distribution of the earthquake hypocenters in 3D defined by earthquake travel-times, and (2) the kinematic compatibility and alignment in 3D of individual nodal planes defined by earthquake first-motions and amplitude ratios.

A simple example of this technique is demonstrated by investigating the seismicity along the San Andreas fault system in the Northern Coachella Valley and along a set of steeply-dipping, blind oblique to predominantly strike-slip *en echelon* faults that occur at depths below about 10 km beneath San Gorgonio Pass. **Figure 4** shows a map view looking NE of this seismicity, together with some of the updated 3D fault models we developed for CFM. This includes the Mission Creek, Banning, and Garnet Hill fault strands, as well as other secondary faults such as the San Gorgonio Pass thrust and the blind Palm Springs fault. The Palm Springs fault represents one of these deep blind, oblique *en echelon* faults. The reason we believe we can confidently identify and map these structures as distinctly separate faults is because of the consistency produced by the hypocenter and nodal plane alignments when looking down-dip or along strike in the plane of slip of each fault.

For example, if we rotate the entire frame of reference of this earthquake and fault volume until we are looking down-dip and in the plane of slip of the Banning strand (**Fig.5**), we see distinctly separate bands of earthquakes along the Mission Creek (red spheres), Banning (yellow spheres), and Garnet Hill faults (purple spheres). The fact that these earthquakes define distinctly different bands at this dip angle indicates that the faults are subparallel. If we continue to rotate the frame of reference until we are looking down-dip and in the plane of slip of the Palm Springs fault (**Fig.6**), the earthquakes along the Palm Springs fault (PSF) now define a very narrow linear trend, as they should if most of the events represent slip along this single principal slip surface. This geometry is also consistent with the geometry of the predominant NW-striking, NE-dipping nodal plane that many of these earthquakes exhibit in their focal mechanism solutions [e.g., *Carena et al.,* 2004]. Moreover, this frame of reference, highlights other faults in this set of deep, *en echelon* strike-slip to oblique slip faults that have remarkably similar NE dips. These faults are in addition to and sub-parallel to the principal slip surfaces of the San Andreas fault zone, and thus help accommodate plate boundary strain through San Gorgonio Pass. This fault set was first identified by *Seeber and Armbruster* [1995] and confirmed by *Carena et al.* [2004], and the resulting 3D fault models developed for CFM (**Figs.4-6**) are virtually identical to previous non-planar 3D fault surfaces independently created using an earlier catalog of relocated focal mechanism solutions and different surface-fitting algorithms [*Carena et al.,* 2004].

Results

For this project and in close collaboration with other members of the CFM Working Group, substantial progress was made on developing new or updated 3D models in several major fault areas, including the onshore Santa Maria basin, Eastern & Western Transverse Ranges, Mojave, various offshore fault systems in the Continental Borderland, and faults within the designated San Gorgonio Pass and Ventura Special Fault Study Areas (SFSA)(**Fig.1**)[*Nicholson et al.,* 2014, 2015; *Plesch et al.,* 2015; *Shaw et al.,* 2015]. These new models expand the lexicon of revised 3D fault

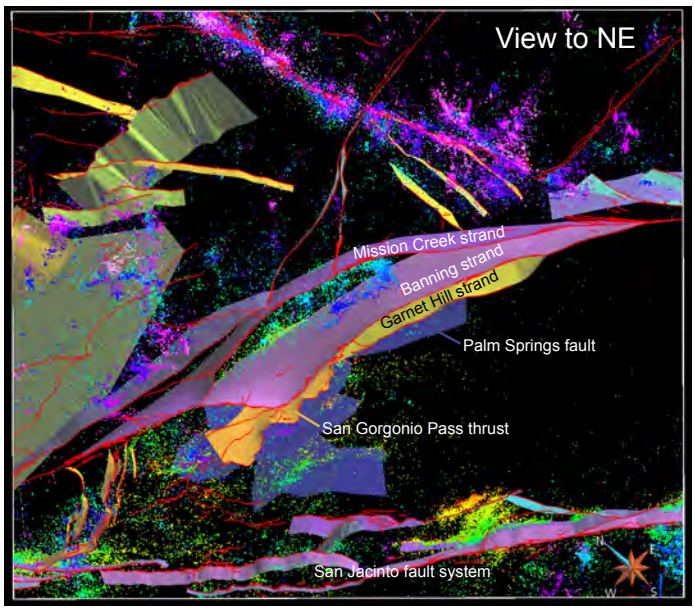

Figure 4. Map view looking NE of San Gorgonio Pass region with seismicity color coded by depth and many of the new, updated 3D fault models developed for CFM. Mission Creek, Banning and Garnet Hill strands typically dip 70° to 80°NE, and each is a distinctly separate, steeply dipping fault to 8-10 km. For clarity, the North Palm Springs fault in the hanging wall of the Banning strand, and the deep detachments below San Gorgonio Pass (**Fig.8**) are not shown. Different interpretations are permissible, e.g., the orange San Gorgonio Pass thrust could be the active up-dip extension of the North Palm Springs fault that has been offset in a right-lateral sense by the more steeply dipping Banning fault strand [e.g., *Seeber and Armbruster,* 1995].

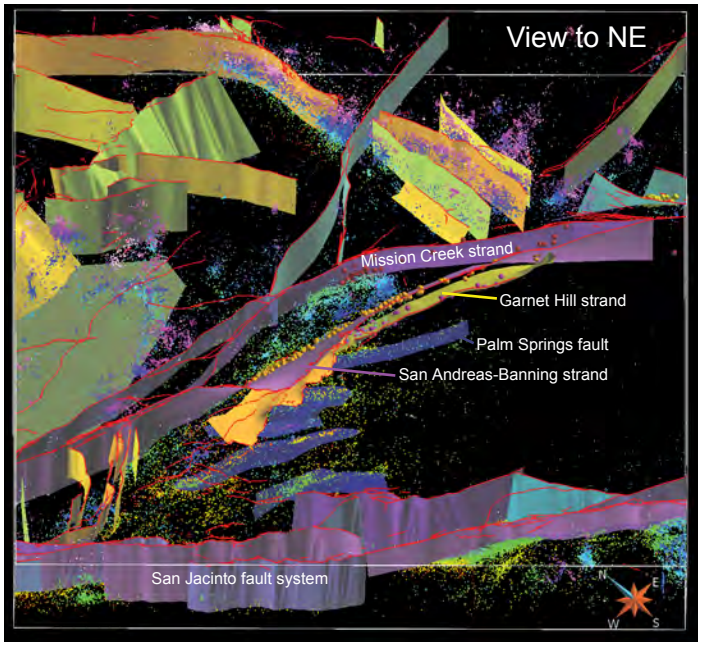

Figure 5. Oblique 3D view looking NE down-dip in the plane of slip of the Banning fault strand in the Northern Coachella Valley. Distinctly different sets of earthquakes that define steeply dipping and subparallel Banning & Garnet Hill faults to depths of ~10 km are highlighted as colored spheres. These subparallel strands correspond to the fault models labeled 1 in the Figure 8 cross section that also shows downdip splays labeled 2 & 3. This seismicity indicates that there are indeed through-going principal slip surfaces at depth that can accommodate dynamic, strike-slip rupture through San Gorgonio Pass. Additional fault models (dark purple), including the Palm Springs fault, represent a set of NW-striking, NE-dipping *en echelon* blind faults at depths >10 km that help accommodate plate boundary slip through San Gorgonio Pass.

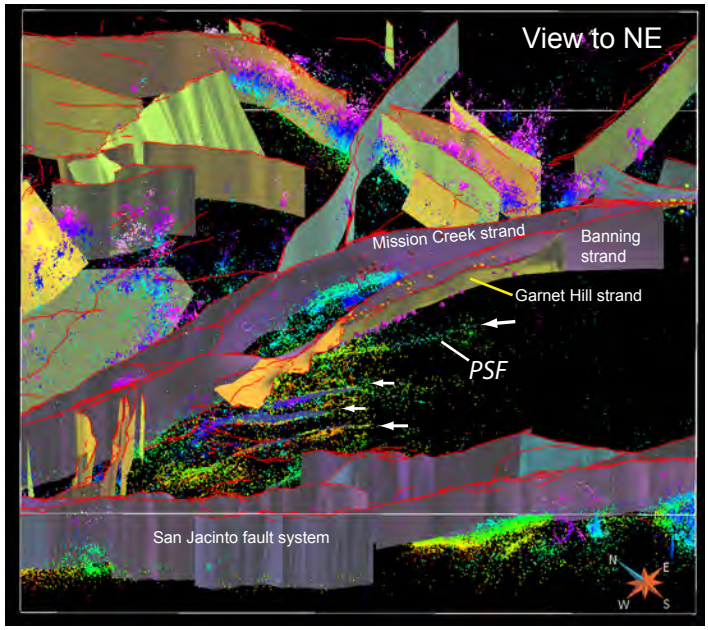

Figure 6. Oblique 3D view of Fig.5 but now looking down-dip of the Palm Springs fault (PSF). Earthquakes along the PSF define a narrow linear trend, as they should if most represent slip along this principal slip surface. Additional faults with similar dips are also revealed by this rotated frame of reference (white arrows). The dark purple fault models represent the set of deep *en echelon* NE-dipping blind faults defined by the linear trends in hypocenter and nodel plane alignments. Several of these fault models in CFM, including the Palm Springs fault, are virtually identical to previous independently derived 3D fault models based on earlier relocated catalogs and different surface-fitting algorithms [*Seeber and Armbruster,* 1995; *Carena et al.,* 2004].

models previously developed for CFM that include the San Andreas fault from Parkfield to San Gorgonio Pass to the Salton Sea, the adjacent sub-parallel Mecca Hills-Hidden Springs fault zone, and the San Jacinto, Elsinore-Laguna Salada, and Agua Tibia-Earthquake Valley fault systems [*Nicholson et al.,* 2011, 2012, 2013]. Several of these earlier CFM fault models were subsequently revised and updated as part of this project based on additional information and after community review and comment. In addition, this project was able to support more detailed focused studies in areas of complex fault geometry, where multiple fault sets and sub-parallel fault zones strongly interact. This included the complex San Gorgonio Pass SFSA along the San Andreas fault, the Ventura SFSA where active onshore and offshore faults and fault-related folds define a complex pattern of 3D deformation, and the Laguna Salada-Indiviso-Sierra Cucapah region at the southern end of the Elsinore-Laguna Salada fault zone. This report will focus on many of these special fault areas, and the recent resulting refinements made to CFM 5.0.

In 2014, many new 3D fault models or alternative representations were added to CFM. In the onshore Santa Maria basin, this included blind and emergent structures such as the Orcutt, Lompoc, Zaca, Los Alamos, Pezzoni-Casmalia, and Santa Ynez Valley faults. In the offshore Borderland, new or updated faults include the Santa Cruz-Catalina Ridge, East Santa Cruz basin, Ferrelo, San Clemente, San Mateo-Carlsbad, San Diego Trough, San Pedro Basin, Descanso, Coronado Bank faults & Coronado Bank detachment. In the Eastern Transverse Ranges, 3D fault models for the Cleghorn, Tunnel Ridge, Pinto Mountain, Morongo Valley, Burnt Mountain-East Wide Canyon, Eureka Peak-West Deception Canyon, and North Frontal Thrust faults were added or updated. In the Western Transverse Ranges, new models were developed for the faults associated with the Southern Frontal fault system (Raymond, Hollywood, Santa Monica, Malibu Coast, Santa Cruz Island, Santa Rosa Island) and the Upper Santa Ana Valley (San Jose, Upland, Walnut Creek, Indian Hill), as well as the Verdugo and Eagle Rock faults. In the Mojave area, new or updated faults include the Lenwood-Lockhart, Helendale-South Lockhart, Pipes Canyon, Barstow trend, Camp Rock, Emerson, Copper Mountain, and faults involved in the Landers and Hector Mine ruptures among others. New or updated CFM fault models were also developed for the Imperial, Dixieland, and West Mesa faults in the Salton Trough, the Kern Canyon fault in the Great Valley area, and several of the many faults, fault splays, and secondary faults associated with the Laguna Salada-Sierra Cucapah-Yuha Desert fault systems (**Fig.1**).

For 2014, specific efforts to improve CFM also focused on developing updated fault sets for the Ventura and San Gorgonio Pass SFSA's. Both San Gorgonio Pass and the Ventura-Santa Barbara area were targeted for integrated, multi-disciplinary investigations as part of the SFSA program [*Yule et al*., 2012; *Dolan et al.,* 2012]. Knowing the subsurface geometry of active faults in these areas is critical for properly modeling seismic rupture or extrapolating near-surface observations to depth, and is particularly important in such complex areas where principal slip surfaces can be multi-stranded, exhibit significant non-planar fault geometry, and intersect or link up with other adjacent major faults. Updated, detailed 3D fault models were also needed in these areas as a basis for integrating, evaluating, and modeling the results from other SFSA investigations.

In the Ventura-Santa Barbara area, new 3D models include a substantially revised set of alternative representations for the North Channel, Pitas Point, Ventura, Red Mountain, Arroyo Parida-Mission Ridge, Santa Ynez, San Cayetano, Oak Ridge and Simi-Santa Rosa faults (**Fig.7**). In the San Gorgonio Pass area, parts of the Crafton Hills complex and other new cross faults near San Bernardino were added, in addition to the Cleghorn and North Frontal Thrust faults. Finally, we attempted to define several new detachment surfaces at mid and deep crustal levels beneath the San Jacinto and San Bernardino Mountains, as part of the San Gorgonio Pass SFSA (**Fig.8**). The net result is that CFM-v5 now contains 90 separate fault zones or distinct fault systems defined by over 300 individual named faults, and 625 primary or alternative fault representations, with 190 new,

updated or revised models added to CFM 5.0 since the release of CFM 4.0 and our previous USGS award [*Nicholson et al,* 2014, 2015; *Plesch et al*., 2014].

Ventura Special Fault Study Area

Figure 7 shows the two sets of alternative interpretations and fault models currently in CFM 5.0 for the Ventura SFSA. The set on the left is from the Harvard group and is based mostly on modeling fault-related fold geometry and well data in the onshore Ventura basin [*Hubbard et al,* 2014]. The set on the right is largely from the UCSB group and based mostly on mapping shallow fault surfaces with industry seismic reflection and well data, and combining this with relocated seismicity in the offshore Santa Barbara Channel [*Kamerling et al*., 2003; *Nicholson and Kamerling*, 1998; *Sorlien et al*., 2012, 2014]. The major difference between these alternative interpretations is the degree to which N-dipping faults, like the Pitas Point, Ventura and Red Mountain faults that merge at depth, remain steeply dipping, or are offset by a near-flat detachment.

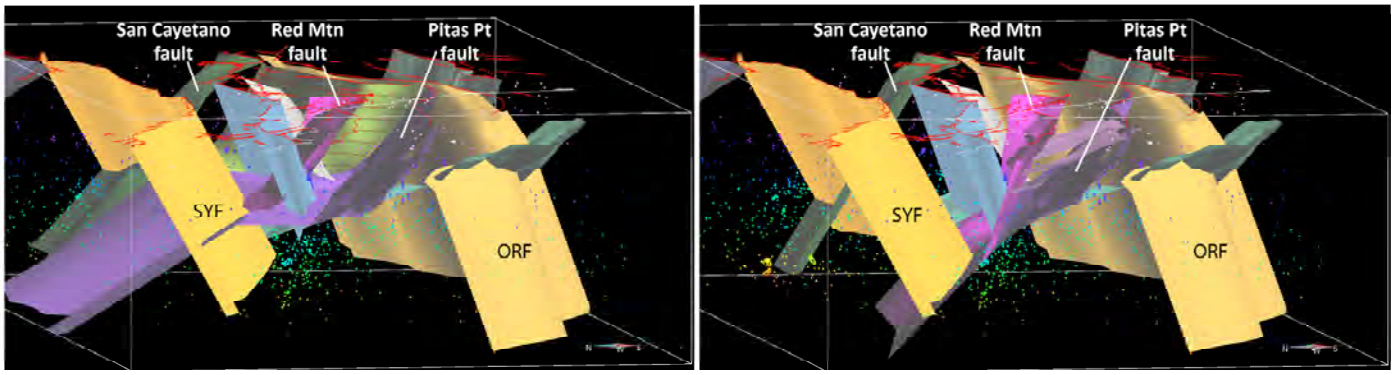

Figure 7. Oblique 3D views looking East of updated faults in the Ventura-Santa Barbara area relative to relocated seismicity (dots) [*Plesch et al*., 2014]. (*left*) CFM 5.0 models with midcrustal detachment from *Hubbard et al* [2014] for Pitas Point, Ventura, Red Mountain, Lion, San Cayetano, and South San Cayetano faults. (*right*) Updated CFM 5.0 models without mid-crustal detachment and steeper dips for the Pitas Point, North Channel, Red Mountain, Arroya Parida-Mission Ridge, San Cayetano and Santa Ynez faults [*Kamerling et al*., 2003; *Nicholson et al*., 2014]. The updated Oak Ridge fault (ORF) is also now a contiguous surface at depth from onshore to offshore.

Geologic evidence for such detachments, or potential slip surfaces, is provided by the presence of the mechanically weak Rincon Shale and other shale layers in younger strata. These mechanically weak layers have facilitated gravity sliding towards the basin from surrounding uplifted areas and subsequent development of significant non-planar 3D fault geometry [*Nicholson et al*., 2007]. In places, these layers are imaged as forming the basal thrust into which some lift-off folds and S-dipping faults, like the Sisar and Padre Juan faults may sole [*Yeats et al*., 1998; *Kamerling et al*., 2003]. Although such detachments may help support the presence of S-dipping out-of-syncline thrust faults or backthrusts, like the Padre Juan fault [*Grigsby,* 1988; *Hopps et al*., 1992], these basin detachments do not seem to strongly influence the major N-dipping basin-bounding faults. **Figure 8** shows an oblique view looking east of the updated North Channel-Pitas Point-Red Mountain fault system [*Kamerling et al*., 2003; *Fisher et al*., 2005] refined for CFM 5.0 using the most recent relocated hypocenter catalog [*Hauksson et al*., 2012], and aftershocks of the 1978 M5.9 Santa Barbara and 2013 M4.8 Isla Vista earthquakes [IV events relocated by *Egill Hauksson*]. The seismicity indicates the shallow faults merge down-dip into a continuous principal slip surface at depth that remains steeply dipping and is not offset by a flat detachment.

The two sets of alternative interpretations for the Ventura basin faults (**Fig.7**) still need to be further tested and evaluated with other data, including seismicity, geodetic strain data & fault slip rates, or by mechanical modeling [*e.g., Marshall et al*., 2014] to see which set best fits the observations and patterns of deformation. They also need to be further updated, refined, and

extended, as they are currently incomplete. CFM 5.0 models for the Ventura-Pitas Point, North Channel and Red Mountain faults only extend west to Coal Oil Point near UCSB. Recent mapping with industry MCS reflection data (*e.g.,* **Fig.2**) now documents, however, that these active fault structures extend past Pt. Conception, a distance of over 120 km [*Sorlien et al.,* 2014].

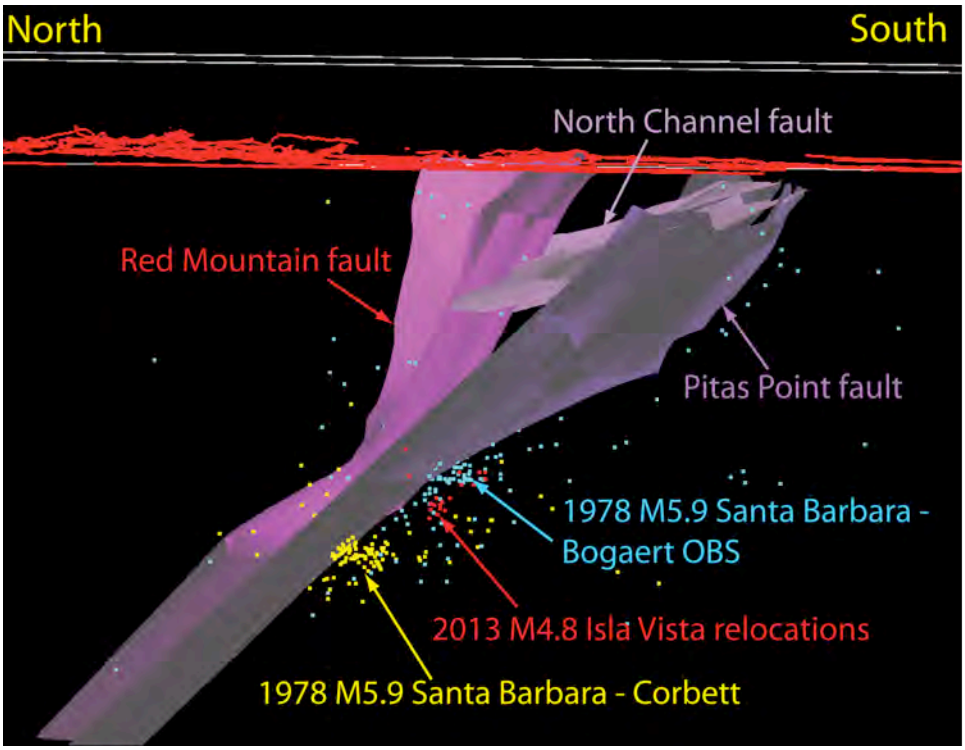

Figure 8. Oblique 3D view looking East of updated and refined CFM 5.0 fault models for the N-dipping North Channel-Pitas Point-Red Mountain fault system, plus relocated aftershocks of the 1978 M5.9 Santa Barbara (blue & yellow) and 2013 M4.8 Isla Vista (red) earthquakes. Most Isla Vista hypocenters are at a depth of ~10-11 km. Isla Vista relocated hypocenters provided by Egill Hauksson (pers.comm., 2013).

San Gorgonio Pass Special Fault Study Area

Along the San Andreas fault proper, there is no place more complex, more enigmatic, or more important to properly understand in 3D than San Gorgonio Pass (SGP)[*Yule,* 2009] and its extension to Cajon Pass where the major San Andreas and San Jacinto fault zones intersect (**Figs.1,3&4**). The geometry and nature of active fault strands in SGP is particularly crucial to resolving the potential for large through-going earthquake rupture, and the resulting strong ground motion predictions for different rupture scenarios of the southern San Andreas fault. Accurate representations of 3D fault surfaces through the Pass are thus not only fundamental to the basic seismic hazard estimation for southern California, but provide the necessary framework for all such future integrated tectonic, geologic, and geophysical studies of this particular fault area.

A major question has always been: what is the geometry of the principal active strand of the San Andreas fault (SAF) through San Gorgonio Pass? **Figure 9** shows an oblique 3D view of updated CFM 5.0 fault representations along the SAF system through San Gorgonio Pass [*Nicholson et al.*, 2013, 2014; *Plesch et al.,* 2014]. In developing these new 3D fault representations, care was taken that fault models were first smoothed to reduce artifacts of model construction, and if the fault extended to surface outcrop, the fault was registered to both DEM and the Qfault surface trace. In this way, 3D models for active strands and down-dip splays of Banning, Garnet Hill, Mission Creek, Mill Creek, San Gorgonio Pass thrust, North Palm Springs, and southern San Andreas faults (SSAF) were created (*e.g.*, **Figs.4,5&10**). Subsequently, faults in the Crafton Hills complex, blind cross faults near San Bernardino, the set of blind *en echelon* faults (**Fig.6**) at depth below SGP (like the Palm Springs fault) and other secondary faults were added, together with representations for the North Frontal Thrust & Cleghorn faults, and for mid- and deep-crustal detachments below the San Jacinto and San Bernardino Mountains (**Fig.9**). These new 3D fault models have already proven

useful to modeling dynamic earthquake rupture along the San Andreas fault through the pass [*Shi et al.,* 2012; *Shi,* 2014], and help define important secondary structures that can strongly influence the seismic behavior, rupture initiation points, and fault slip rates along the San Andreas fault itself [*e.g., Nicholson et al.,* 1986; 2012*; Nicholson,* 1996; *Herbert and Cooke*, 2012]

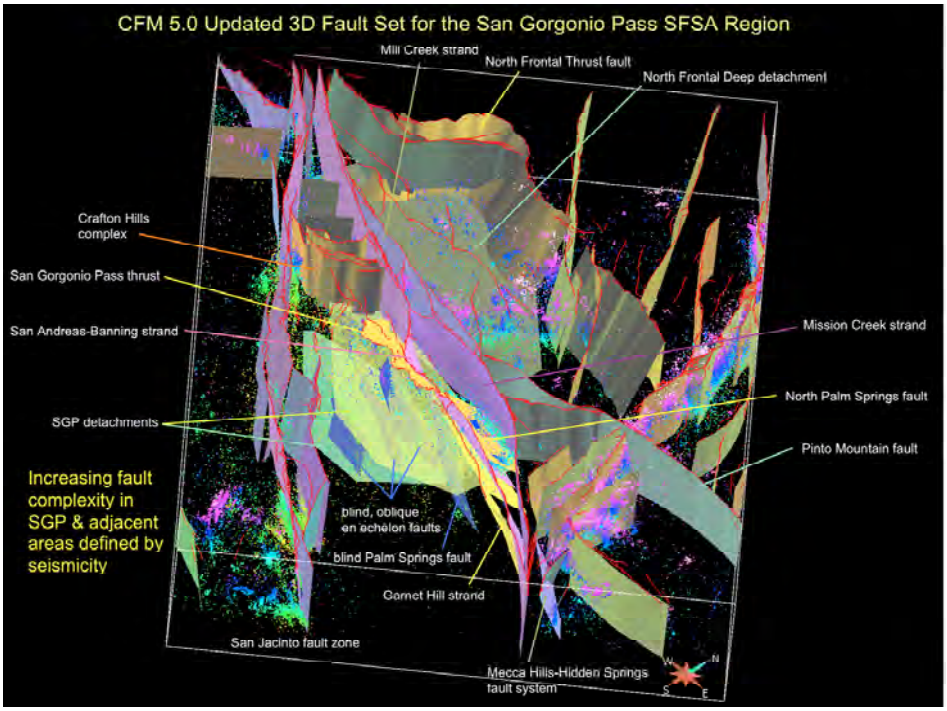

Figure 9. Oblique view looking NW of CFM 5.0 fault models for the San Andreas fault system through San Gorgonio Pass (SGP) [*Nicholson et al.,* 2014; *Plesch et al.,* 2014]. The presence of the through-going Banning fault strand at depth increases the possibility of dynamic rupture through SGP [*Shi,* 2014], while the Crafton Hills complex may affect SAF slip rates [*Herbert*, 2012]. New CFM faults for 2014 include parts of the Crafton Hills comples & other blind cross faults, additional blind oblique *en echelon* faults, North Frontal Thrust & Cleghorn faults, and mid- and deep-crustal detachments below the San Jacinto and San Bernardino Mountains.

The principal observation from the seismicity is that there is indeed an active, steeply dipping through-going SAF-Banning fault through SGP. Other major faults, including the Garnet Hill and Mission Creek strands are also steeply-dipping to depths of ~8-10 km (**Figs.5&10**). These steeply dipping fault strands intersect, merge or splay down-dip with a set of moderately-dipping oblique thrust faults, including the North Palm Springs fault, located in the hanging wall of the Banning fault strand (**Fig.10**). This interpretation of a through-going, steeply dipping SAF, and one or more moderately dipping oblique thrust faults in its hanging-wall is not new. Both *Seeber and Armbruster* [1995] and *Carena et al*. [2004] were able to identify nearly identical fault structures based on the alignment of relocated hypocenters and focal mechanism nodal planes. This fault geometry is also not surprising as it is very similar to the geometry of the San Andreas fault through the Santa Cruz Mountains, where similar oblique motion is again partitioned between a near-vertical SAF, and a more moderately dipping oblique dip-slip fault that produced the 1989 Loma Prieta earthquake [*Seeber and Armbruster,* 1990]. The new, more extensive relocated earthquake catalogs we used for CFM 4.0 and 5.0 basically reaffirm this earlier interpretation. The only difference is that in CFM, we distinguish between the shallow San Gorgonio Pass thrust fault that is largely defined by surface geologic mapping, and the deeper North Palm Springs fault defined by seismicity to emphasize that these two fault sections are defined by different data sets, and that this structure, if continuous, appears to be offset horizontally in a right-lateral sense by the through-going Banning fault strand. In previous interpretations, the North Palm Springs fault would be simply labeled as the down-dip extension of the San Gorgonio Pass thrust [*e.g., Seeber and Armbruster,* 1995; *Carena et al.,* 2004]. This is a very viable, reasonable interpretation and as such both alternative representations are included in CFM. It is thus reassuring that recent imaging results from the Salton Sea Imaging Project (SSIP) in the northern Coachella Valley confirm that the Banning and Garnet Hill faults are indeed steeply dipping and sub-parallel to 8-10 km [*Fuis et al.,* 2014], and are distinctly separate from the North Palm Springs fault, as has been modeled in CFM since 2011 (*e.g.*, **Fig.10**).

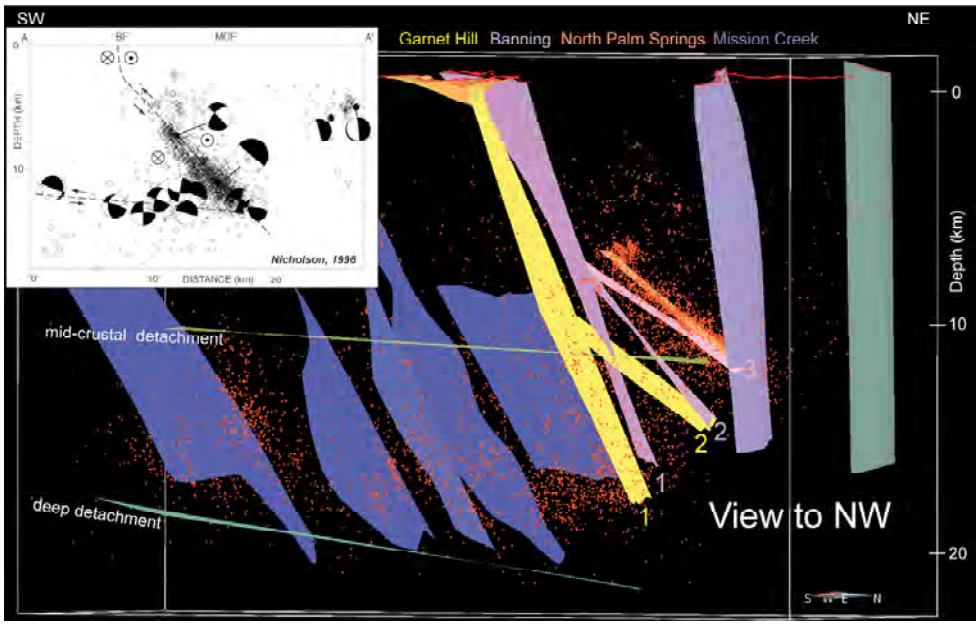

Figure 10. Cross section view looking NW along the Banning & Garnet Hill CFM fault strands [*Nicholson et al.,* 2014]. The faults can remain steeply dipping and subparallel to depths >10 km (model 1), they can splay down-dip (model 2), or do both to merge and interact with faults involved in the 1986 North Palm Spings sequence (e.g., model 3) [*Nicholson et al.,* 2010]. (*inset*) Similar cross section showing hypocenters & focal mechanisms that define the North Palm Springs fault (orange) and top mid-crustal detachment (green).

The new 3D fault models developed for CFM thus help characterize a more complex pattern of fault interactions at depth between various fault sets, while providing more continuous, steeply dipping and smoothly varying rupture surfaces through San Gorgonio Pass. These more complete, detailed, and more complex multiple 3D fault models may help explain some of the more enigmatic fault behavior and patterns of deformation that may be otherwise difficult to understand. For example, the failure of the 1986 North Palm Springs mainshock to develop into a full-scale rupture of the SSAF could be the result of it occurring primarily on the adjacent secondary North Palm Springs fault (**Fig.10**), rather than on what might be considered the primary, more steeply dipping through-going Banning fault strand (Option #1, **Fig.10**). Moreover, the decrease in slip rate observed SE along strike of the San Bernardino strand of San Andreas fault in San Gorgonio Pass may be related to adjacent secondary faults, like the Crafton Hills complex [*Herbert and Cooke,* 2012] and to slip being more distributed as the fault becomes multi-stranded at depth (**Fig.9**), rather than changing geometry of a single fault as was once believed [*Dair and Cooke,* 2009].

Southern San Andreas and Mecca Hills-Hidden Springs fault zones

In constructing 3D fault models for CFM, special care was taken to distinguish between sub-parallel fault strands or secondary fault systems. For example, in CFM 5.0, two, closely-spaced adjacent fault systems are mapped and modeled in the Coachella Valley: a near-vertical Southern San Andreas fault (SSAF) and a moderately NE-dipping Mecca Hills-Hidden Springs fault (MH-HSF)(**Fig.11**). The MH-HSF is an active NE-dipping sub-parallel structure adjacent to the SSAF that is responsible for the bulk of the seismicity located east of the SSAF surface trace. Previous investigators have inferred that this seismicity may be produced by a dipping SSAF that dips NE at about 65° [e.g., *Fuis et al.,* 2007] based mainly on the projection of seismicity alignments near Salt Creek [*Lin et al.,* 2007]. However, further study of this seismicity, clearly shows that this NE-dipping principal slip surface strikes oblique to the SSAF surface trace and progressively projects to crop out kilometers farther east as one moves north [*Nicholson et al.,* 2010]. The primary basis for modeling these as two separate fault systems is: 1) their separate known mapped surface traces, 2) their distinctly separate displacement histories, and 3) their earthquake populations at depth that define distinctly separate near-vertical and NE-dipping fault surfaces with their hypocenter and focal mechanism nodal plane alignments (**Fig.11**). A recent SSIP fault-crossing profile does image the complete geometry of the MH-HSF as modeled in CFM [*Fuis et al.,* 2014], however, no similar fault-plane reflections were found associated with the mapped SSAF surface trace.

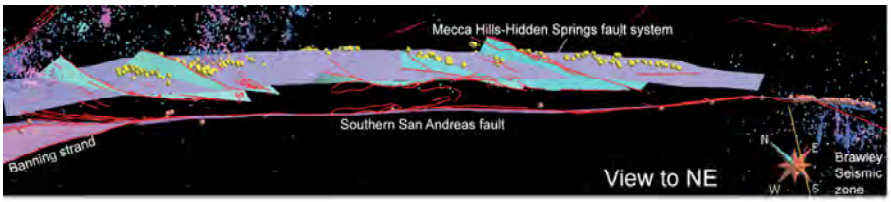

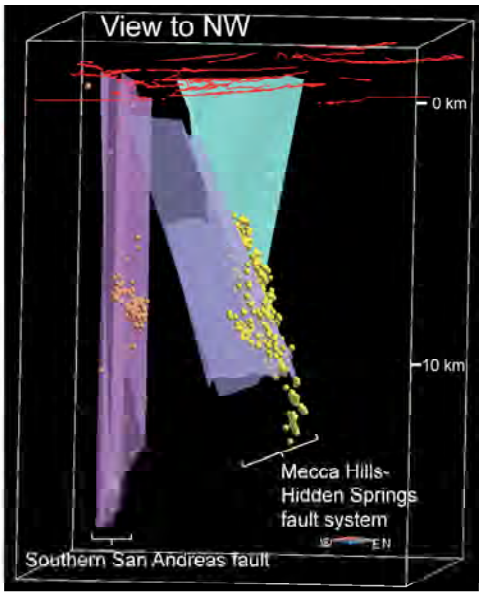

Figure 11. (*top*) Map view looking NE of the near-vertical Southern San Andreas and adjacent, subparallel NE-dipping Mecca Hills-Hidden Springs fault systems. Earthquakes at depth associated with each separate fault system are highlighted as orange and yellow spheres, respectively. (*right*) Cross section 3D view looking NW along these two separate near-vertical and NE-dipping fault systems [*Nicholson et al*., 2014]. The separate mapped faults and earthquake hypocenter and nodal plane alignments are consistent with two distinct adjacent fault systems, similar to other fault system pairs found elsewhere (*e.g*., Laguna Salada-Sierra Cucapah, Banning-North Palm Springs, and San Andreas-Loma Prieta).

The presence of both a dipping MH-HSF system and a vertical or near-vertical SSAF has significant implications. First, it can help explain observations that are otherwise difficult to reconcile. For example, a few scattered deep earthquakes do occur directly beneath the SSAF surface trace, seismic reflection data along the SSAF suggest a steep to near vertical fault [*Rymer et al,* 2012; *Catchings et al*., 2012; *Goldman et al*., 2012] and, as shown in **Fig.11**, the SSAF is clearly vertical at Bombay Beach where it intersects the Brawley Seismic Zone based on earthquake and nodal plane alignments [*Nicholson et al*., 2010; 2014]. However, geodetic data along the SSAF indicate that maximum shear strain is displaced about 7 km NE of the SSAF surface trace [*Fialko,* 2006]. This could be the result of the active NE-dipping MH-HSF working in combination with a vertical SSAF, rather than shear strain only accumulating on what would otherwise be an inferred NE-dipping SSAF. The presence of two active fault systems side-by-side implies, however, that some plate motion is already being diverted from the SSAF onto the Eastern California shear zone as far south as Bombay Beach, and not necessarily only at the Indio Hills where the southernmost end of the Landers-Joshua Tree sequences begin to splay off from the main SSAF system.

Laguna Salada and Sierra Cucapah faults, and the 2010 El Mayor-Cucapah sequence

Besides developing updated 3D fault models along major mapped surface traces (e.g., **Fig.1**), substantial effort was also made to develop preliminary 3D fault models for several major recent earthquake ruptures. For CFM 4.0, this included fault models for the 1971 San Fernando, 1979 Imperial Valley, 1986 North Palm Springs, 1987 Elmore Ranch-Superstition Hills, 1992 Landers-Joshua Tree, 1994 Northridge, 1999 Hector Mines, and 2010 El Mayor-Cucapah earthquakes. The 2010 M7.2 El Mayor-Cucapah earthquake was particularly complex [*Hudnut et al*., 2010; *Kroll et al*., 2012], and demonstrated that major earthquakes can occur on adjacent sub-parallel fault systems in close proximity to previous large earthquakes on distinctly separate structures (e.g., 1892 M7 Laguna Salada earthquake). Preliminary CFM 4.0 fault models for the Sierra Cucapah faults, active cross faults in the Yuha Desert and for the adjacent Laguna Salada fault system were developed based on initial aftershock hypocenters and mapped fault surface traces [*Hauksson et al*., 2011; *Fletcher et al*.,2010; *Treiman et al*., 2010]. These models were subsequently revised, updated and improved based on a more integrated analysis of the later relocated aftershocks [*Hauksson et al*., 2012], updated near-surface geologic mapping and InSAR studies of fault surface traces [e.g., *Oskin et al*., 2011, 2012; *Teran et al*., 2011], and following comment and review of the preliminary versions.

The updated 3D models for CFM 5.0 include fault representations for the Borrego, Pescadores, Paso Superior, Paso Inferior, and Sierra Cucapah, adjacent dipping strands and fault splays of the Laguna Salada-Indiviso fault system, and various associated cross faults like Painted Gorge Wash, Devil's Canyon, Yuha Well, Shell Beds, Yuha Wash, Yuha, and El Mayor-Cucapah cross faults (**Fig.12**). In constructing these new 3D models, we distinguished between the predominantly steep to East-dipping shallow faults and related fault splays that we correlate to the major, deep East-dipping Sierra Cucapah fault, and the predominantly steep to West-dipping strands and down-dip splays related to the Laguna Salada fault. Numerous cross faults and other secondary faults were triggered by the 2010 event. Many of these correlated well with mapped surface fault traces (**Fig.13**), while others remained blind, such as the Yuha Wash fault.

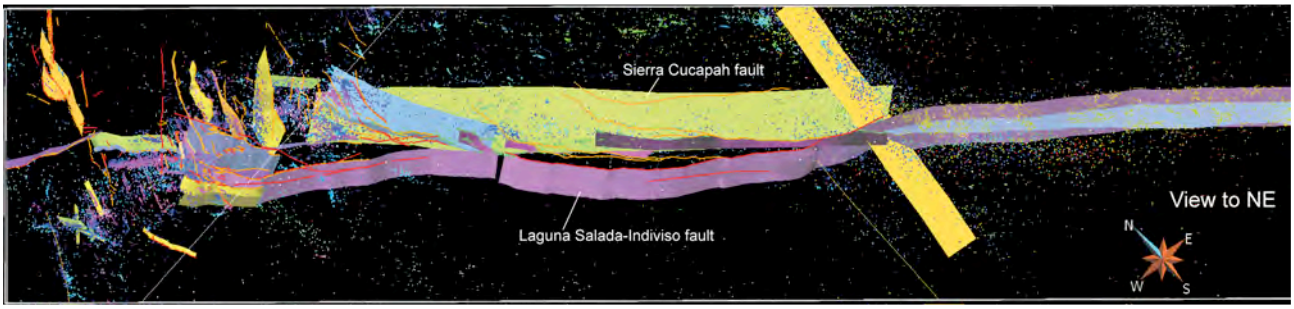

Figure 12. Oblique 3D view looking East across various updated CFM 3D fault representations for the 2010 M7.2 El Mayor-Cucapah rupture and its associated aftershocks [*Nicholson et al*., 2014]. CFM 5.0 3D fault models were developed for the steep to East-dipping Pescadores, Borrego, Paso Superior, Paso Inferior, deep Sierra Cucapah and related fault splays, for the steep to West-dipping Indiviso, Laguna Salada and other related faults, and for a number of curved to planar cross faults, including the Painted Gorge Wash, Devil's Canyon, Yuha Well, Shell Beds, Yuha Wash, Yuha, and various other cross faults in teh Yuha Desert. Relocated aftershock hypocenters from *Hauksson et al*. [2012]; mapped fault surface trace data courtesy of Ken Hudnut, John Fletcher and Jerry Treiman.

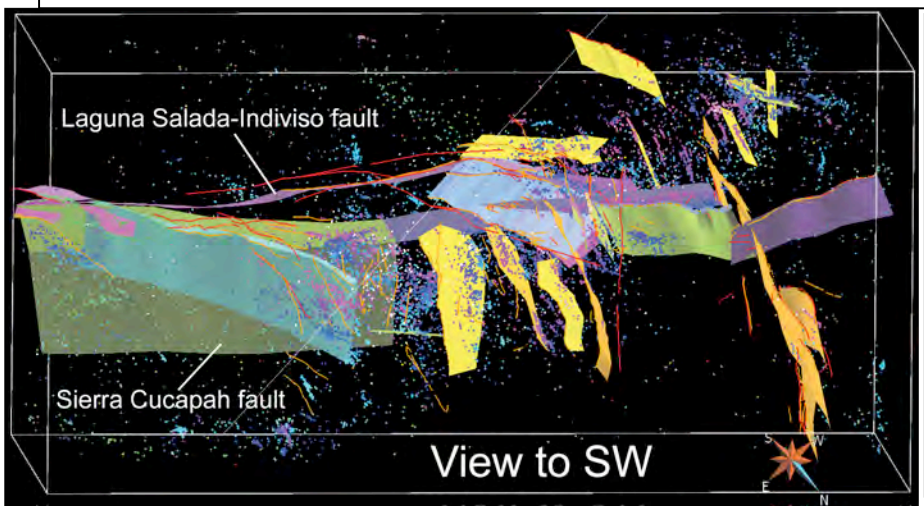

Figure 13. Oblique 3D view looking SW to West across the northern end of the El Mayor-Cucapah sequence and slightly down-dip of the W-dipping Laguna Salada fault. Aftershocks illuminate deeper sections of various fault splays and cross faults, many of which exhibited surface rupture, but others remained blind, such as the Yuha Wash fault [*Nicholson et al*., 2014; *Plesch e al*., 2014].

Reorganization of the CFM fault database

In collaboration with Andreas Plesch and other members of the CFM Working Group, the CFM fault database was reorganized with a new hierarchical name and numbering scheme. This reorganization allows CFM to properly organize, name and number the increasing variety and complexity of modeled, multi-stranded principal slip surfaces, adjacent secondary faults, and alternative fault representations that have been or will be developed for CFM, while maintaining a greater consistency with fault nomenclature from the CGS Fault Activity database. The new CFM

database naming scheme provides unique identifiers (including number, name and abbreviation) for each level of the fault hierarchy under which a particular fault segment is classified. Levels of hierarchy include Fault Area, Fault Zone or System, Fault Section, Fault Name, Fault Strand or Model, and Fault Component. With CFM 5.0, we have also now added qualifiers for the author (e.g., YULE, SHAW, FUIS, etc.) and CFM version number (CFM4, CFM5) for when the particular fault model or alternative representation was introduced. These additional hierarchical levels allow for more flexible database searches and easier identification of fault components, and possible system-level associations of individual 3D fault elements that comprise CFM that may help identify related faults or linked fault systems capable of potential larger earthquake ruptures.

Conclusions

For this project, significant and substantial improvements were made to CFM for Version 5.0. These improvements include new, more complex and updated 3D fault surfaces (**Fig.1**) based on detailed fault surface trace, industry well, seismic reflection, relocated hypocenter and focal mechanism nodal plane data, and an updated fault database with an improved hierarchical fault naming and numbering system. Alignments of relocated earthquake hypocenters and focal mechanism nodal planes were typically used to define the subsurface 3D geometry of active faults at deeper levels, and to construct updated digital 3D fault representations for CFM (**Fig.1**). These new models allow for more non-planar, multi-stranded 3D fault geometry, including changes in dip and dip direction along strike and down dip, based on the changing patterns of earthquake hypocenter and focal-mechanism nodal plane alignments, rather than projecting faults to depth assuming a constant (often vertical) dip and dip direction, as was the case for many of the earlier preliminary fault models in CFM. These complex fault surfaces are often best resolved when looking in 3D down-dip or along strike within the plane of slip for each fault (**Figs.5,6,10&11**).

The results document a wide variety of complex fault deformation styles, including: various aspects of strain partitioning and fault-related folding; sets of both high-angle and low-angle faults that mutually interact; blind and emergent structures; significant non-planar, multi-stranded faults with variable dip along strike and with depth; and active mid-crustal detachments at different structural levels. In places, closely-spaced fault strands or fault systems can remain surprisingly subparallel to seismogenic depths, while in other areas, major strike-slip to oblique-slip faults can merge or diverge with depth. The updated CFM 3D fault surfaces thus help characterize a more complex pattern of fault interactions at depth between various fault sets and linked fault systems, and a more complex fault geometry than typically inferred or expected from projecting near-surface geologic or geophysical data down-dip.

In 2014, the formally reviewed and ranked CFM 4.0 and its rectilinear version were released, along with an initial CFM Version 5.0. In addition to continuing to update older fault models, many new faults or alternative representations were added to CFM 5.0 that were not represented in any previous CFM model versions. The net result is that CFM 5.0 now contains 90 separate fault zones or distinct fault systems defined by over 300 individual named faults, with 325 new, updated, or revised fault models or alternative representations added to CFM since Version 3.0.

Data and Product Availability

The primary earthquake datasets used for this research are available from the SCEC Data Center (http://data.scec.org/research-tools/altcatalogs.html). Most mapped fault surface trace data we used were provided by the California Geological Survey primarily through the USGS Quaternary Fault and Fold database website (http://earthquake.usgs.gov/hazards/qfaults/). Products and updated digital representations of 3D fault surfaces generated by this project are available from the SCEC Community Fault Model website (http://structure.rc.fas.harvard.edu/cfm/modelaccess.html).

Related Publications, Reports and Outreach Presentations

De Hoogh, G.L., C. Nicholson, C.C. Sorlien, and R.D. Francis, Structure and Evolution of the Eastern Boundary of the California Outer Continental Borderland, *Seismological Research Letters*, **86**, n.2B, p.735 (2015).

Hauksson, E., C. Nicholson, J.H. Shaw, A. Plesch, P.M. Shearer, D.T. Sandwell and W. Yang, Refined views of strike-slip fault zones, seismicity, and state of stress associated with the Pacific-North America plate boundary in Southern California, *Eos (Transactions of AGU),* **94** (52), Abstract T21E-05 (2013).

Nicholson, C., Continuing to Evaluate 3D Fault Geometry in Special Fault Study Areas and to Improve the SCEC Community Fault Model (CFM), *2013 SCEC Annual Report,* n.13108, 7 pp (2014).

Nicholson, C., Updating Active 3D Fault Geometry in Special Fault Study Areas and Improving the SCEC Community Fault Model (CFM), *2014 SCEC Annual Report,* n.14015, 8 pp (2015).

Nicholson, C., A. Plesch and E. Hauksson, Active 3D fault geometry along the San Andreas fault system through San Gorgonia Pass inferred from seismicity and other data, SCEC San Gorgonio Pass Special Fault Study Area Workshop, *2014 SCEC Annual Meeting Program,* p.4 (2014).

Nicholson, C., A. Plesch, C.C. Sorlien, J.H. Shaw and E. Hauksson, The SCEC 3D Community Fault Model (CFM Version 5.0): An updated and expanded fault set of oblique crustal deformation and complex fault interaction for southern California, *Eos (Transactions of AGU),* **95** (52), Abstract T31B-4584 (2014).

Nicholson, C., A. Plesch, C.C. Sorlien, J.H. Shaw and E. Hauksson, The SCEC Community Fault Model Version 5.0: An updated and expanded 3D fault set for southern California, *2015 Pacific Section AAPG Joint Meeting Program,* p.77, Oxnard, CA (2015).

Plesch, A., C. Nicholson, C. Sorlien, J.H. Shaw and E. Hauksson, SCEC Community Fault Model Version 5.0, *2014 SCEC Annual Meeting Proceedings & Abstracts,* **XXIII,** p.171 (2014).

Shaw, J.H., A. Plesch, C. Tape, M.P. Suess, T. Jordan, G. Ely, E. Hauksson, J. Tromp, T. Tanimoto, R. Graves, K. Olsen, C. Nicholson et al., Unified Structural Representation of the southern California crust and upper mantle, *Earth & Planetary Science Letters,* **415**, p.1-15 (2015).

Sorlien, C.C., J.T. Bennett, M.-H. Cormier, B.A. Campbell, C. Nicholson and R.L. Bauer, Late Miocene-Quaternary fault evolution and interaction in the Southern California Inner Continental Borderland, *Geosphere*, 11, n.4, doi:10.1130/GES01118.1 (2015).

Sorlien, C.C, C. Nicholson, R.J. Behl et al., The geometry of the post-Miocene North Channel-Pitas Point fault system including post-Miocene folding, Santa Barbara Channel, California, *2014 SCEC Annual Meeting Proceedings & Abstracts,* **XXIV**, p.180 (2014).

Sorlien, C.C, C. Nicholson, R.J. Behl, C.J. Marshall and J. Kennett, The Quaternary North Channel-Pitas Point Fault System in Northwest Santa Barbara Channel, California, *Eos (Transactions of AGU)*, **95** (52), Abstract T34A-07 (2014).

Non-technical Summary

Detailed analysis of well-determined earthquake locations and focal mechanisms, together with other datasets like industry seismic reflection and well data, are used to define the 3D geometry of active subsurface faults and to create new or improved, updated digital 3D fault surfaces for the

SCEC Community Fault Model (CFM) Version 5.0. Many new faults or alternative representations were added to CFM 5.0 that were not represented in any previous CFM model versions. This included faults in the onshore Santa Maria basin, Eastern and Western Transverse Ranges, Mojave, various offshore fault systems, and faults within the designated San Gorgonio Pass and Ventura Special Fault Study Areas. The net result is that CFM 5.0 now contains 90 separate fault zones or distinct fault systems defined by over 300 individual named faults, with 325 new, updated, or revised fault models or alternative representations added to CFM since Version 3.0. These new models allow for more non-planar, multi-stranded 3D fault geometry, including changes in dip and dip direction along strike and down dip, based on the changing patterns of earthquake hypocenter and focal-mechanism nodal plane alignments. These new CFM fault surfaces describe a more complex pattern of interacting fault sets at depth accommodating crustal deformation in southern California, and have already provided the basis for improved dynamic earthquake rupture models, variable fault slip rate models, and correlations with associated regional topography.

References

Bennett, J., C.C. Sorlien, et al., Quaternary deformation of the Newport-Inglewood-Carlsbad-Coronado Bank-Descanso Fault System: Long Beach to San Diego, California, *2012 SCEC Annual Meeting Proceedings & Abstracts*, **XXII**, p.90 (2012).

Bryant, W. A. (compiler), 2005, Digital Database of Quaternary and Younger Faults from the Fault Activity Map of California, version 2.0: accessed July 2010 from California Geological Survey Web Page, http://www.consrv.ca.gov/cgs/information/publications/Pages/QuaternaryFaults_ver2.aspx.

Bullard, T.F. and W.R. Lettis, 1993, Quaternary fold deformation associated with blind thrust faulting, Los Angeles basin, California, *J. Geophys. Res.*, **98**, p. 8349–8369.

Carena, S., J. Suppe and H. Kao, Lack of continuity of the San Andreas fault in southern California: Three-dimensional fault models and earthquake scenarios, *J. Geophys. Res,* **109**, doi:10.1029/2003JB002643, B04313, 17 pp (2004).

Catchings, R.D.; G. Fuis; M.J. Rymer; M. Goldman et al., Salton Seismic Imaging Project Line 6: San Andreas Fault and Northern Coachella Valley Structure, Riverside and San Bernardino Counties, California, *Eos (Trans. AGU)*, **v.93**, n.52, abstract T51B-2583, Fall meeting, 2012.

Dair, L. and M.L. Cooke, San Andreas fault geometry through the San Gorgonio Pass, California, *Geology*, **37**, n.2, p.119-122 (2009).

Davis, T.L., J. Namson and R.F. Yerkes, 1989, A cross section of the Los Angeles area: Seismically active fold and thrust belt, the 1987 Whittier Narrows earthquake, and earthquake hazard, *J. Geophys. Res.*, **94**, p. 9644–9664.

De Hoogh, G.L., C. Nicholson, C.C. Sorlien and R.D. Francis, Neogene Basin and Plate Boundary Development in the Outer Continental Borderland Offshore Southern California, *Eos (Transactions of AGU)*, **90**(52), Abstract T13C-1891 (2009).

Dolan, J.F., J.H. Shaw and T.K. Rockwell, The Ventura Region Special Fault Study Area: Towards an understanding of the potential for large, multi-segment thrust ruptures in the Transverse Ranges, *2012 SCEC Annual Meeting Proc. & Abstracts*, **XXII**, p.99-100 (2012).

Fattaruso, L. and M. Cooke The influence of complex fault geometry on uplift patterns in the Coachella Valley and Mecca Hills of Southern California, *2012 SCEC Annual Meeting Proc. & Abstracts*, **XXII**, p.102 (2012).

Fattaruso, L.A., M.L. Cooke, R.J. Dorsey and B.A. Housen, Mechanical insights into tectonic reorganization of the southern San Andreas fault system since ca. 1.5 Ma, *2012 SCEC Annual Meeting Proc. & Abstracts*, **XXII**, poster 105, p.140 (2014).

Fialko, Y., Interseismic strain accumulation and earthquake potential on the southern San Andreas fault system, *Nature,* **441**, p.968-971 (2006).

Fisher, M.A., W.R. Normark, H.G. Greene, H.J. Lee and R.W. Sliter, Geology and tsunamigenic potential of submarine landslides in Santa Barbara Channel, Southern California, *Marine Geology*, **224**, p.1-22 (2005).

Fletcher, J.M, T.K. Rockwell, et al., Distribution and kinematics of surface ruptures associated with the El Mayor-Cucapah earthquake, *2010 SCEC Annual Meeting Proceedings & Abstracts*, **XX**, p.213-214 (2010).

Fuis, G.S., D. Scheirer, V. Langenheim and M. Kohler, The San Andreas fault in southern California is almost nowhere vertical—Implications for tectonics, *2007 SCEC Annual Meeting Proc. & Abstracts*, **XVII**, p.112 (2007).

Fuis, G.S., K. Bauer, et al., Geometry of the San Andreas fault and sedimentary basin in the northern Salton Trough, *2014 SCEC Annual Meeting Proc. & Abstracts*, **XXIV**, poster 092, p.141 (2014).

Goldman, M.; G. Fuis; R.D. Catchings; M.J. Rymer et al., Salton Seismic Imaging Project Line 7: Data and Analysis to Date, *Eos (Trans. AGU)*, **93**, n.52, abstract T51B-2581, Fall meeting, 2012.

Grigsby, F.B., Structural development and the Ventura Avenue anticlinal trend at the San Miguelito and Rincon oil fields, Ventura County, California, in *Santa Barbara and Ventura Basins: Tectonics, Structure, Sedimentation, Oilfields Along an East-West Transect,* A.G Sylvester and G.C. Brown, eds., *Coast Geological Survey Guidebook 64*, p. 111-124 (1988).

Hardebeck, J.L. and P.M. Shearer, Using S/P amplitude ratios to constrain the focal mechanisms of small earthquakes, *Bull. Seismol. Soc. Am.*, **v.93**, n.6, p.2434–2444 (2003).

Hauksson, E., Understanding seismicity in the context of complex fault systems and crustal geophysics, *2012 SCEC Annual Meeting Proc. & Abstracts*, **XXII**, p.108 (2012).

Hauksson, E. and P. Shearer, Southern California hypocenter relocation with waveform cross-correlation; Part 1, Results using the double-difference method, *Bull. Seismol. Soc. Am.*, **v.95**, n.3, p.893-903, 2005.

Hauksson, E., W. Yang and P. Shearer, Waveform relocated earthquake catalog for Southern California (1981 to June 2011), *Bull. Seismol. Soc. Am.,* **v.102,** n.4, p.2239-2238, doi:10.1785/0120110241, 2012.

Hauksson, E., J. Stock, K. Hutton, W. Yang, J. A. Vidal-Villegas and H. Kanamori, The 2010 Mw 7.2 El Mayor-Cucapah Earthquake Sequence, Baja California, Mexico and Southernmost California, USA: Active Seismotectonics along the Mexican Pacific Margin, *Pure Appl. Geophys.*, **168**, p. 1255–1277, 2011.

Herbert, J., The role of fault complexity and secondary faults on fault slip, *SCEC Special Fault Study Area Workshop on San Gorgonio Pass,* June, 2012.

Herbert, J. and M. Cooke, 2012, Sensitivity of the Southern San Andreas fault system to tectonic boundary conditions and fault configuration, *Bull. Seismol. Soc. Am.,* **102,** p.2046-2062, doi:10.1785/0120110316.

Hester, R.J. and J.N. Truex (1977). San Cayetano fault field trip, *AAPG Pacific Section Guidebook*, 35 pp.

Hopps, T.E., H.E. Stark, and R.J. Hindle, *Subsurface geology of Ventura Basin, California, Ventura Basin Study Group Report*, 45 pp., 17 structure contour maps and 84 structure panels comprising 21 cross sections, Rancho Energy Consultants, Inc., Santa Paula, CA, 1992.

Hopps, T.E., H.E. Stark, R.J. Hindle, J.H. Thompson, and G.C. Brown, CS30: Correlated section across Central Ventura Basin from T5N/R19W to T1N/R18W, California, *Pacific Section–Am. Assoc. Petrol. Geol. Cross Section*, April, 1995.

Hubbard, J., Structural linkage of onshore and offshore thrust systems across the Ventura fault and prospects for large earthquakes in the Transverse Ranges, *SCEC Annual Meeting Proc. & Abstracts*, **XXI**, p.7, 2011.

Hubbard, J., J.H. Shaw, J.F. Dolan, T.L. Pratt, L. McAuliffe and T. Rockwell, Structure and seismic hazard of the Ventura Avenue anticline and Ventura fault, California: Prospect for large, multisegment ruptures in the Western Transverse Ranges, *Bull. Seismol. Soc. Am.*, 104, n.3, doi:10.1785/0120130125 (2014).

Hudnut, K.W., J.M. Fletcher et al., Earthquake rupture complexity evidence from field observations, *Eos (Transactions of AGU)*. **91** (52), Abstract T51E-02 (2010).

Hudnut, K., L. Seeber and J. Pacheco, Cross-fault triggering in the November 1987 Superstition Hills earthquake sequence, southern California, *Geophys. Res. Lett.*, **16**, p. 199–202, 1989.

Huftile, G. and R.S. Yeats, Convergence rates across a displacement transfer zone in the western Transverse Ranges, Ventura basin, California, J. Geophys. Res., v. 100, p. 2043–2068 (1995).

Kamerling, M. and C. Nicholson, The Oak Ridge fault and fold system, Eastern Santa Barbara Channel, California, *1995 SCEC Annual Report*, **v. II**, p. C26–C30 (1996).

Kamerling, M.J., C.C. Sorlien, and C. Nicholson (1998), Subsurface faulting and folding onshore and offshore of Ventura basin: 3D map restoration across the Oak Ridge fault, *SCEC 1998 Annual Meeting Report*, **V**, p.68-69.

Kamerling, M.J., C.C. Sorlien and C. Nicholson (2003), 3D development of an active oblique fault system, northern Santa Barbara Channel, California, *Seismol. Res. Lett.*, **v. 74**, n.2, p. 248.

Kamerling, M. J., Sorlien, C. C., Archuleta, R., and Nicholson, C., 2001, Three-dimensional geometry and interactions of faults and structures along the northern margin of the Santa Barbara Channel, California: *Geol. Soc. Am. Abstracts with Prog.,* **v. 33,** no. 3, p. A-41.

Kroll, K., E. Cochran, K.B. Richards-Dinger and D.F. Sumy, Complex fault interaction in the Yuha Desert, *Eos (Trans. AGU)*, **v.93**, n.52, abstract S13B-05, Fall meeting, 2012.

Lees, J. M., Geotouch: Software for Three and Four-Dimensional GIS in the Earth Sciences, *Computers & Geosciences*, 1999.

Lindsey, E.O, V.J. Sahakian, Y. Fialko, Y. Bock and T.K. Rockwell, Space geodetic investigation of interseismic deformation along the San Jacinto fault: Effects of heterogeneous elastic structure and fault geometry, *Seismological Research Letters*, **v.83**, n.2, p. 434, 2012.

Lin, G., P. M. Shearer, and E. Hauksson, Applying a three-dimensional velocity model, waveform cross-correlation, and cluster analysis to locate southern California seismicity from 1981 to 2005, *J. Geophys. Res.*, **v.112**, n.B12, 14 pp, B12309, doi:10.1029/2007JB004986, 2007.

Lozos, J.C. and D.D. Oglesby, Seemingly minor details of fault geometry may strongly affect rupture propagation, *Seismol. Res. Lett.,* **83**, n.2, p.370, 2012.

Marshall, C.J., C. Sorlien, C. Nicholson, R.J. Behl and J.P. Kennett, Sedimentation in an active fold and thrust belt, Santa Barbara Basin, California: Local and regional influences on the spatial and temporal evolution of sedimentation from 1.0 Ma to Present, *AAPG National Meeting,* Long Beach, CA (2012).

Marshall, S.T., M.L. Cooke and S.E. Owen, Interseismic deformation associated with three-dimensional faults in the greater Los Angeles region, California, *J. Geophys. Res.*, **114**, n.B12, B12403 (2009).

Marshall, S.T., G.J. Funning and S.E. Owen, Fault slip rates and interseismic deformation in the western Transverse Ranges, California, *J. Geophys. Res,* **v.118**, p.4511-4534, doi:10.1002/jgrb.50312 (2013).

Marshall, S.T., G.J. Funning and S.E. Owen, The distribution of fault slip rates in the Ventura fault system, CA, *2014 SCEC Annual Meeting Proceedings & Abstracts*, **XXIII**, poster 093, p.161 (2014).

Meade, B.J. and B.H. Hager, Block models of crustal motion in southern California constrained by GPS measurements, J. Geophys. Res., 110, B03403, doi:10.1029/2004JB003209 (2005).

Mori, J., D. Wald and R. Wesson, Overlapping fault planes of the 1971 San Fernando and 1994 Northridge, California earthquakes, Geophys. Res. Lett., 22, n.9, p.1033-1036, 1995.

Nicholson, C., Seismic behavior of the San Andreas fault in the Northern Coachella Valley, California: Comparison of the 1948 and 1986 earthquake sequences, *Bulletin of the Seismological Society of America,* **v.86**, n. 5, p. 1331-1349 (1996).

Nicholson, C., E. Hauksson, A. Plesch and P. Shearer, Resolving 3D fault geometry at depth along active strike-slip faults: Simple or complex?, *2008 SCEC Annual Meeting Proceedings & Abstracts*, **XVIII**, p.143-144 (2008).

Nicholson, C., E. Hauksson, and A. Plesch, Revised 3D fault models for the Southern San Andreas fault system extending from San Gorgonio Pass to the Salton Sea, *Pacific Section AAPG-GSA Cordilleran Joint Meeting Abstracts w/Program*, **v.42**, n.4, Abstract 21-8, p.69, Anaheim, CA (2010).

Nicholson, C., E. Hauksson and A. Plesch, Active fault geometry and crustal deformation along the San Andreas fault system through San Gorgonio Pass, California: The view in 3D from seismicity, *Eos (Transactions of AGU)*, **93** (52), Abstract T22C-03 (2012).

Nicholson, C. and M.J. Kamerling, Reliability of 2D kinematic fold models to infer deep fault structure in the western Transverse Ranges, California, *Proceedings of the NEHRP Conference and Workshop on the Northridge, California Earthquake of January 17, 1994*, **v. II**, p. 299–306 (1998).

Nicholson, C., M.J. Kamerling, C.C. Sorlien, T.E. Hopps and J.-P. Gratier, Subsidence, compaction and gravity-sliding: Implications for 3D geometry, dynamic rupture and seismic hazard of active basin-bounding faults in southern California, *Bull. Seismol. Soc. Am.*, **97**, n.5, p.1607-1620 (2007).

Nicholson, C., A. Plesch, J. Shaw, E. Hauksson and P. Shearer, Improvements in SCEC Community Fault Model for Version 4.0, *UCERF-3 California Statewide Fault Model & Paleoseismic Workshop*, Pomona, CA (2011).

Nicholson, C., A. Plesch, J.H. Shaw and E. Hauksson, Upgrades and improvements to the SCEC Community Fault Model: Increasing 3D fault complexity and compliance with surface and subsurface data, *2012 SCEC Annual Meeting Proceedings & Abstracts*, **XXII**, p.125-126 (2012).

Nicholson, C., L. Seeber, P. Williams and L.R. Sykes. Seismicity and fault kinematics through the eastern Transverse Ranges, California: Block rotations, strike-slip faulting and low-angle thrusts, *Journal of Geophysical Research*, **91**, p. 4891-4908, (1986).

Nicholson, C., L. Seeber, P. Williams and L.R. Sykes. Seismic evidence for conjugate slip and block rotation within the San Andreas fault system, southern California, *Tectonics*, **5**, p. 629-648 (1986).

Nicholson, C., C.C. Sorlien, C.S. Schindler, and G. DeHoogh, Large vertical motions and basin evolution in the Outer Continental Borderland off Southern California associated with plate boundary development and continental rifting, Eos (Transactions of AGU), 92 (52), Invited Abstract T31F-04 (2011).

Oglesby, D.D. and P.M. Mai, Fault geometry, rupture dynamics and ground motion from potential earthquakes on the North Anatolian Fault under the Sea of Marmara, *Geophys. J. Inter.,* **v.188**, n.3, p.1071-1087 (2012).

Olsen, K.B, S.M. Day, et al., Strong shaking in Los Angeles expected from southern San Andreas earthquake, *Geophys. Res. Lett.*, **33,** L07305, doi:10.1029/2005GL025472, 4pp (2006).

Oskin, M.E., J.R. Arrowsmith, et al., Near-field coseismic deformation quantified from differential airborne LiDAR of the El Mayor-Cucapah earthquake surface rupture, *2011 SCEC Annual Meeting,* **XXI**, p.210 (2011).

Oskin, M.E. J.R. Arrowsmith, et al., Near-field deformation from the El Mayor-Cucapah earthquake revealed by differential LiDAR, *Science,* v.335, n.6069, p. 702-705 (2012).

Plesch, A., C. Nicholson, J.H. Shaw, E. Hauksson and P.M. Shearer, New developments for the SCEC Community Fault Model and its associated fault database, *2010 SCEC Annual Meeting Proceedings & Abstracts*, **XX**, p.261-262 (2010).

Plesch, A., J. Shaw et. al., Community Fault Model (CFM) for Southern California, *Bulletin of the Seismological Society of America*, **v.97**, n.6, p.1793–1802, doi: 10.1785/0120050211 (2007).

Redin, T., J. Forman and M.J. Kamerling, 2005, Santa Barbara Channel structure and correlation sections, Pacific Section AAPG Cross Sections CS-32 through CS-42, Bakersfield, CA.

Richards-Dinger, K.B. and W.L. Ellsworth, A comparison of earthquake (Re)Location methods *Seismol. Res. Lett,* **v.72**, n.2, p. 229 (2001).

Rockwell, T., Large co-seismic uplift of coastal terraces across the Ventura Avenue Anticline: Implications for the size of earthquakes and the potential for tsunami generation, *2011 SCEC Annual Meeting Proceedings & Abstracts*, **XXI**, p.7 (2011).

Rockwell, T., K. Wilson, L. Gamble, M. Oskin, and E. Haaker, Great earthquakes in the western Transverse Rages of southern California on the Pitas Point-Ventura thrust system, 5th International INQUA Meeting on Paleoseismology, Active Tectonics and Archeoseismology (PATA), Busan, Korea (2014).

Ryan, K.J., E.L. Geist, M. Barall and D.D. Oglesby, Dynamic models of earthquakes and tsunamis from rupture on the Pitas Point and lower Red Mountain faults offshore Ventura, California, *Seismological Research Letters,* **86**, n.2b, p.666 (2015).

Rymer, M.J.; G. Fuis; R.D. Catchings; M. Goldman et al., Salton Seismic Imaging Project Line 5—the San Andreas Fault and Northern Coachella Valley Structure, Riverside County, California, *Eos (Trans. AGU)*, **v.93**, n.52, abstract T51B-2584, Fall meeting, 2012

Seeber, L. and J. Armbruster, The San Andreas fault system through the Transverse Ranges as illuminated by earthquakes, *J. Geophys. Res*, **100**, p. 8285-8310 (1995).

Seeber, L., J.G. Armbruster, and P. Geiser, The 1994 Northridge and 1971 fault ruptures and surrounding seismogenic faults as illuminated by small earthquakes, *Geol. Soc. Am. Abstracts w/Prog.*, **v. 33**, n.3, p.A-63 (2001).

Schindler, C.S., C. Nicholson and C. Sorlien, 3D Fault Geometry and Basin Evolution in the Northern Continental Borderland Offshore Southern California, *Eos (Trans. AGU)*, **88**, n.52, T32A-1100 (2007).

Shaw, J.H. and P.M. Shearer, An elusive blind-thrust fault beneath metropolitan Los Angeles, *Science,* **v.283**, p. 1,516-1,518, 1999.

Shaw, J. H., and J. Suppe (1996). Earthquake hazards of active blind-thrust faults under the central Los Angeles basin, California, *J. Geophys. Res.* **101**, 8623-8642.

Shearer, P., E. Hauksson and G. Lin, Southern California hypocenter relocation with waveform cross-correlation, Part 2 Results using Source-specific station terms and cluster analysis, *Bull. Seismol. Soc. Am.*, **v.95,** n.3, p.904-915, 2005.

Shi, Z. and S.M. Day, Studying the effect of fault roughness on strong ground motion, *Seismol. Res. Lett.*, **81**, n.2, p.311, 2010.

Shi, Z., S. Ma, S.M. Day and G.P. Ely, Dynamic rupture along the San Gorgonio Pass section of the San Andreas fault, *Seismol. Res. Lett.*, **83**, n.2, p. 423, 2012.

Sorlien, C.C, B.A. Campbell, W.S. Alward, L. Seeber. M.R. Legg, and M. Cormier, Transpression along strike-slip restraining segments vs regional thrusting in the Inner California Continental Borderland, *2009 SCEC Annual Meeting Proceedings & Abstracts*, **XIX**, p.264-265 (2009).

Sorlien, C. C., J. P. Gratier, B. P. Luyendyk, J. S. Hornafius, and T. E. Hopps, Map restoration of folded and faulted late Cenozoic strata across the Oak Ridge fault, onshore and offshore Ventura basin, California, *Geol. Soc. America Bull.*, **v. 112**, p. 1080-1090, 2000.

Sorlien, C. C., and Kamerling, M. J., 2000, Fault displacement and fold contraction estimated by unfolding of Quaternary strata, onshore and offshore Ventura basin, California, *Final Report to U.S. Geological Survey NEHRP,* contract 99HQGR0080.

Sorlien, C. C., M. J. Kamerling, L. Seeber, and K. G. Broderick (2006), Restraining segments and reactivation of the Santa Monica–Dume–Malibu Coast fault system, offshore Los Angeles, California, J. Geophys. Res., 111, B11402, doi:10.1029/2005JB003632.

Sorlien, C.C, C.J. Marshall, C. Nicholson et al., Post-1 Ma deformation history of the anticline forelimb above the Pitas Point-North Channel fault in Santa Barbara Channel, California, *2012 SCEC Annual Meeting Proceedings & Abstracts*, **XXII**, p.139-140 (2012).

Tarnowski, J.M. and D.D. Oglesby, Dynamic models of potential earthquakes in the San Gorgonio Pass, CA, *Eos (Transactions of AGU)*, **93** (52), Abstract S21B-2519 (2012).

Teran, O.J., J.M. Fletcher, T.R. Rockwell, K.W. Hudnut, M.E. Oskin, et al., Structural controls on the surface rupture associated with the M7.2 El Mayor-Cucapah earthquake: A comparative analysis of scarp array kinematics, orientation, lithology and width, *2011 SCEC Annual Meeting,* **XXI**, p. 236-237 (2011).

Treiman, J.A. K.J. Kendrick, M.J. Rymer, and E.J. Fielding, Fault rupture in the Yuha Desert, California, from the El Mayor-Cucapah earthquake, and the contribution of InSAR imagery to its documentation, 2*010 SCEC Annual Meeting Proceedings and Abstracts,* **XX**, p.284 (2010).

Trugman, D.T., and E.M. Dunham, A 2D pseudo-dynamic rupture model generator for earthquakes on geometrically complex faults, *2013 SCEC Annual Meeting Proceedings & Abstracts*, **XXIII**, p.151 (2013).

Tsutsumi, H. and R.S. Yeats, Tectonic setting of the 1971 and 1994 Northridge earthquakes in the San Fernando Valley, California, *Bull. Seismol. Soc. Am.*, **v.89**, n.5, p. 1,232-1,249 (1999).

U.S. Geological Survey and California Geological Survey, 2006, Quaternary fault and fold database for the United States, accessed July 2010 from USGS web site: http://earthquake.usgs.gov/hazards/qfaults/.

Wright, T.L., 1991, Structural geology and tectonic evolution of the Los Angeles basin, California, in *Active Tectonic Basins*, T.K. Biddle, ed., *AAPG Memoir* **52**, p.35-134.

Yeats, R.S.. Late Cenozoic structure of the Santa Susana fault zone, in *Recent Reverse Faulting in the Transverse Ranges, California, USGS Professional Paper*, **1339**, p. 137-160, 1987.

Yeats, R.S., Neogene tectonics of the East Ventura and San Fernando Basins, in *Geology and Tectonics of the San Fernando Valley and East Ventura Basin, California,* T.L. Wright and R.S. Yeats, eds, *Pacific Section AAPG Guidebook*, **GB77**, p. 9-36, 2001.

Yeats, R.S. and G.J. Huftile (1995). Oak Ridge fault system and the 1994 Northridge, California, earthquake, *Nature,* **v.373**, p. 418–420.

Yeats, R.S., G.J. Huftile, and L.T. Sitt, Late Cenozoic tectonics of the east Ventura basin, California, *Am. Asoc. Petrol. Geol. Bull.,* **v. 78**, p.1040-1074, 1994.

Yeats, R.S., Late Quaternary slip rate on the Oak Ridge Fault, Transverse Ranges, California: Implications for seismic risk, *Journal of Geophysical Research*, v. **93**, p. 12,137-12,149, 1988.

Yule, D., Research Focus: The enigmatic San Gorgonio Pass, *Geology*, **37**, n.2, p.191-192 (2009).

Yule, D, M.L. Cooke and D. Oglesby, SCEC Workshop on San Gorgonio Pass: Structure, stress, slip, and the likelihood of through-going rupture, *2012 SCEC Annual Meeting Proc. & Abstracts*, **XXII**, p.75 (2012).

Yule, D. and K. Sieh, Complexities of the San Andreas fault newar San Gorgonio Pass: Implications for large earthquakes, J. Geophys. Res., 109, n.B11, 2548, doi:10.1029/2001JB000451 (2003).